Tribology International 185 (2023) 108575

Contents lists available at ScienceDirect

Tribology International

journal homepage: www.elsevier.com/locate/triboint

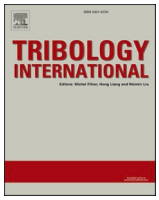

Towards a deeper understanding of temperature-dependent material removal of single-crystal AlN: An atomistic study

Jian Guo [a], Yang Liu [a], Lingfeng Duan [a], Fengling Zhang [b], Chen Xiao [b,c,*]

[a] School of Mechanical Engineering, University of South China, Hengyang 421001, Hunan Province, PR China
[b] Advanced Research Center for Nanolithography (ARCNL), Science Park 106, 1098XG Amsterdam, the Netherlands
[c] Van der Waals-Zeeman Institute, Institute of Physics, University of Amsterdam, Science Park 904, 1098XH Amsterdam, the Netherlands

ARTICLE INFO

Keywords:
Molecular dynamics simulation
AlN
Temperature dependent nanowear
Wear coefficient

ABSTRACT

Temperature-dependent material attrition and subsurface lattice damage of single-crystal AlN at various scratching depths/forces are investigated at atomic level using molecular dynamics simulation. An ultimate removal precision of depth down to monolayer of AlN is achieved based on the present temperature-dependent critical conditions. The number of worn atoms, positively influenced by temperature due to the reduction of hardness, increases exponentially with increasing normal force in the plastic domain. Archard-type wear coefficient K values calculated at different temperatures increase linearly with normal force, and the slope is independent of temperature. Independently of load and temperature, a wear coefficient normalized with the tangential contact area, K/A_{tang}, is developed to interpret the removal efficiency of AlN substrate with diamond abrasive.

1. Introduction

Sliding contact between solid surfaces leads to material detaching, a process known as material removal or wear is a ubiquitous phenomenon and has attracted widespread interest in surface processing and mechanical component applications across scales [1–3]. In particular, controlling and modeling the material removal volume/rate is of significance in the fields of ultra-precision surface finishing and nano-devices due to the size effect when the dimension drops dramatically to sub-/nanoscale [4–7]. According to the well-known Archard wear equation, material removal volume V is predicted empirically to be proportional to the applied normal force F_n and the sliding distance L, while being inversely proportional to the hardness of the relatively weaker contacting surface H [8,9]:

$$V = K\frac{F_n L}{H} \tag{1}$$

where K is the wear coefficient, which in the case of abrasive wear depends on the shape factor and the penetration parameters of an asperity [10,11]; in the case of adhesive wear, it is a function of the local shear strength and the corresponding geometry at the contact interface [12,13]. In experimental conditions the hardness of the topmost layer of material in the contact may not be known with any certainty; consequently, the ratio $w_s = K/H$ known as the dimensional wear coefficient or the specific wear rate is more useful. However, available models with physical meaning were not found to explain the observed variation in values of w_s, which varies from 10^{-2} to 10^{-10} mm^3/N·m [8]. This long-standing problem has remained unresolved, and evaluation of the wear coefficient is still relying on empirical data, with no insight from a physical model.

To precisely control and simulate the material removal process in actual applications, the removal mechanism was studied experimentally at nanoasperity contact in which the atomic force microscopy (AFM) probe was employed to rub the flat workpiece with certain applied normal force, velocity/contacting time, sliding track/distance, and environmental conditions [14–16]. The threshold contact pressure for removing brittle material surfaces, such as Si, GaAs, GaN, and AlN, is close to its hardness value, below which there is no material loss and protrusion-type damage occurs due to friction/pressure-induced amorphization beneath the wear area [17]. In the plastic contact region, material removal behavior dominated by plastic deformation is following the Archard-type equation (Eq. 1), which suggests that the removal volume exhibits a nearly linear relationship as a function of external normal force, sometimes is proportional to the work done by

* Corresponding author at: Advanced Research Center for Nanolithography (ARCNL), Science Park 106, 1098XG Amsterdam, the Netherlands.
E-mail addresses: C.Xiao@arcnl.nl, xiaochenswjtu93@gmail.com (C. Xiao).

https://doi.org/10.1016/j.triboint.2023.108575
Received 6 December 2022; Received in revised form 1 May 2023; Accepted 4 May 2023
Available online 5 May 2023

the friction forces as described by Reye's hypothesis [18]. Above critical pressure value is reduced dramatically when tribochemistry or tribocorrosion is introduced at the sliding interface with the assistance of external force [19,20]. In this case, the material removal rate cannot be plotted as a function of external load according to an Archard-type but increases exponentially with increasing contact pressure as the material is removed via pressure/stress-assisted tribochemical reactions which obey the empirical Arrhenius equation [21]. However, the removal behavior and mechanism of brittle materials are challenging to describe precisely due to limited experimental and characterization techniques. Molecular dynamics (MD) simulation is widely used as an effective theoretical simulation to dynamically manipulate the internal structural deformation and transformation under various mechanical inputs and thereby to reveal the material removal process at the atomic scale [22,23].

Temperature is of great importance in the material removal process across scales, which contributes to adhesive or abrasive removal by reducing the surface hardness, and tribochemical removal by lowering the activation energy of chemical reactions that occurs at the tribological interface [24–27]. In actual friction and wear processes, the temperature distribution of contact area is very complicated under the influence of many factors, such as environmental temperature/media, sliding velocity, normal force, counter-surface, surface topography, the thermal conductivity of friction pair materials, and the distribution of temperature field in each contact point is not uniform and is extremely difficult to quantify [28–33]. That is the reason why empirical results always hardly reflect the real temperature-dependent material removal behavior and the underlying mechanism is still poorly understood. By employing the MD method to characterize the material removal process at sphere-flat contact in different uniform temperature fields, it is straightforward to not only model the abrasive wear behavior of brittle material surface but also to construct a physical wear model under ideal conditions to explicate the intrinsic physical meaning of the wear coefficient [9].

As a promising wide-bandgap semiconductor material, wurtzite aluminum nitride (wz-AlN) has a potential application in nanoelectronic and optoelectronics devices, which require the AlN substrates with sub-nanometer surface roughness and global geometric accuracy [34–39]. To date, the lack of understanding of the material-removal mechanism involved at the nanoscale to the atomic scale has limited the further optimization of the processing of AlN and fulfillment of surface quality requirements in the semiconducting industry.

To simulate the single asperity contact during the material removal process in ultra-precision surface finishing, in this work, a nanoscale diamond abrasive was used to scratch the monocrystalline AlN workpiece through MD simulation under the presence of the different temperature fields. The atomic-scale mechanical removal behavior, elastic-plastic transition mechanism, interfacial frictional force, the evolution of subsurface crystal distortion, and the relationship between these properties and applied normal force/scratching depth in various temperature conditions were investigated, respectively. In the plastic region, the variation in scratching hardness of the topmost layer of AlN substrate in the contact with diamond nano abrasive was estimated as a function of external normal force and environmental temperature based on the MD simulation of the dynamics contact evaluation during of nanoscratching process. Subsequently, K was mathematically fitted according to the Archard-type equation (Eq. 1) and Reye's assumption, suggesting that it is actually an intrinsic characteristic of the material and temperature independent. Furthermore, the results indicate that temperature does not govern the removal mechanism of AlN material, and the linear increase of K in the plastic region is mainly attributed to the increased contact area which is approximately linear to the applied normal force.

2. Method

The scratching MD model of nanoscale diamond abrasive against wz-AlN(0001) workpiece and their basic configuration in detail have been described in the previous literature [10]. We used Vashishta potential [40] to function the interatomic interactions within the AlN workpiece and Lenard-Jones potential to function the interactions between the diamond abrasive and the AlN workpiece. Hereinto, the parameters of the L–J potential for C—Al and C—N pairs are listed in Table 1.

Langevin thermostat [41] was applied to the thermostat layer to realize the designed environmental temperature and dissipate the indentation and scratching-induced heat. To comprehensively investigate the influence of temperature on surface nanotribological and subsurface structural properties, we performed the scratching simulation at a wide range of temperatures (100–1000 K) using various scratching depths of 4–36 Å. Periodic boundary conditions were applied in the x- and y-directions to eliminate the size effect. Before the scratching process, the simulation system was sufficiently relaxed in a canonical ensemble (NVT) for 30 ps. The entire indentation and scratching processes were simulated in a microcanonical ensemble (NVE). Crucial simulation parameters are listed in Table 2. Dislocation extraction algorithm (DXA) [42], Identify Diamond Structure (IDS) [43], and coordination number (CN) calculation methods were combined to analyze the structural transformation of wz-AlN from the atomic scale to the nanoscale. An open-source large-scale atomic/molecular massively parallel simulator (LAMMPS) was employed to execute the MD simulation; The OVITO [44] software (version 2.9.0) was used to realize the visualization of simulation data and further analyze the structural features.

3. Results and discussion

3.1. Temperature dependence of force, contact areas, and hardness

Fig. 1a—c shows the evolutions of normal force (F_n), tangential force (F_t), and coefficient of friction (COF) with scratching distance d varied from 0 to 140 Å; Notes that plots showing the effect of temperature on the evolution of these forces in the entire scratching process using all selected scratching depths are placed in Supplementary Figs. S1–S3. The first ~20 Å in scratching distance was the onset regime in which the simulation system changed from the indentation mode to the scratching mode. F_n decreased in the onset regime and then leveled off with a certain fluctuation with increasing d; the decrease in F_n was ascribed that during scratching the rear part of the diamond abrasive gradually lost contact with the AlN workpiece and led to a reduction in normal contact area (see Fig. 2a). F_t also demonstrated a similar onset behavior and the increase in F_t during onset regime was primarily due to the occurrence of wear with the pile-up forming in front the scratching diamond abrasive. Notes that F_n at 1200 K increased evidently when d exceeded ~100 Å, which should be related to a server structural change in the subsurface of the AlN workpiece.

Fig. 1d—f displays the averaged F_n, F_t, and COF over the stable scratching process (d = 20–140 Å) as a function of h. F_t increased linearly with h at almost every temperature, and the higher the temperature, the lower the rate of increase in F_t. With the designed h ranging from 4 to 36 Å, the AlN workpiece experienced elastic deformation, elastic-plastic transition, plastic deformation, and ductile-brittle transition in sequence regardless of temperature. As long as h was small enough, the AlN surface exhibited ultralow F_t for each temperature because the elastic

Table 1
L–J potential parameters of C–Al and C–N interactions.

Parameter	C–Al	C–N
σ (Å)	3.6920	3.3678
ε (meV)	7.4456	3.7204

Table 2
Simulation parameters.

Parameter	Values	
Dimensions (Å)	Size of AlN workpiece: 350 × 250 × 150	Radius of diamond abrasive: 4
Initial temperature, T (K)	100, 300, 500, 800, 1200	
Scratching velocity, v (m/s)	40	
Time step (fs)	1	
Scratching direction	[1–210] crystal orientation	
Scratching distance, d (Å)	0–140	
Scratching depth, h (Å)	4, 8, 10, 12, 16, 20, 24, 28, 32, 36	

deformation dominated the scratching process. As h increased enough to cause plastic deformation of AlN, F_t increased linearly with h for each temperature, and increasing temperature can reduce the increasing rate of F_t, as shown in Fig. 1e. Also, Fig. 1d indicates that F_n increased linearly first and then logarithmically, and level off finally. For a given h, the higher the temperature, the higher the F_n in the elastic stage, but the lower the F_n in the plastic and ductile-fracture transition stage. For instance, F_n for different temperatures of 100, 300, 500, 800, and 1200 K at $h = 36$ Å are approximately 1176, 1043, 1029, 999, and 821 nN, respectively. COF increased with the increase of h for each temperature and the higher the temperature, the greater the COF, as shown in Fig. 1f. The slight increase in COF with temperature indicated that F_t did not decrease as strongly with temperature as F_n.

To analyze the influence of temperature on the contact pressure during scratching, the contact area should be determined first. In this study, the normal contact area (A_{norm}) and tangential contact area (A_{tang}) were calculated according to Eqs. 2 and 3 [10,45,46], respectively.

$$A_{norm} = \pi\sigma^2 \sum_{i \in contact} \cos\alpha_i \tag{2}$$

$$A_{norm} = \pi\sigma^2 \sum_{i \in contact} \cos\alpha_i \sin\theta_i \tag{3}$$

Where σ is atom radius, α_i denotes the angle under which the contact atom i is seen from the center of the spherical abrasive, and θ_i denotes the angle under which atom i is seen with respect to the scratch direction. The evolutions of A_{norm} and A_{tang} with d for a given $h = 20$ Å shown in Fig. 2a and b suggest that increasing the temperature can result in more severe fluctuations in contact area. Evolutions of A_{norm} and A_{tang} with d for all selected scratching depths are plotted in Supplementary Figs. S4 and S5. The averaged A_{norm} and A_{tang} over the stage scratching stage as a function of h for different temperatures are shown in Fig. 2c and d, respectively. The normal contact area experienced different regimes according to the scratching-induced deformation of AlN: with the increase in temperature, the normal contact area increased rapidly during the elastic stage, increased more slowly in the plastic stage, and decreased sharply once the ductile-brittle transition of AlN occurred. The slight increase in tangential contact area was due to the increase in pile-up caused by the rise of temperature.

Further, the contact pressure can be determined from the force and the contact area of the diamond abrasive against the AlN workpiece. Correspondingly, a normal contact pressure (P_{norm}) and a tangential (or called transverse) contact pressure (P_{tang}) were distinguished and calculated according to Eqs. 4 and 5, respectively.

$$P_{norm} = \frac{F_n}{A_{norm}} \tag{4}$$

$$P_{tan\ g} = \frac{F_t}{A_{tan\ g}} \tag{5}$$

Fig. 3a and b show the evolutions of P_{norm} and P_{tang} with d using a constant scratching depth of $h = 20$ Å for different temperatures, suggesting at this scratching depth the contact pressure could be reduced by temperature. The entire curves for all the selected scratching depths can be found in Supplementary Figs. S6 and S7. The averaged values of P_{norm} and P_{tang} over the stage scratching process ($d = 20$–140 Å) as a function of h for each temperature are displayed in Fig. 3c and d. In the elastic stage, the contact area increased with the increase in temperature for the same scratching depth. As the plastic deformation becomes more and more violent, the contact area decreased with the increase in temperature. According to the deformation situation, the variation of contact

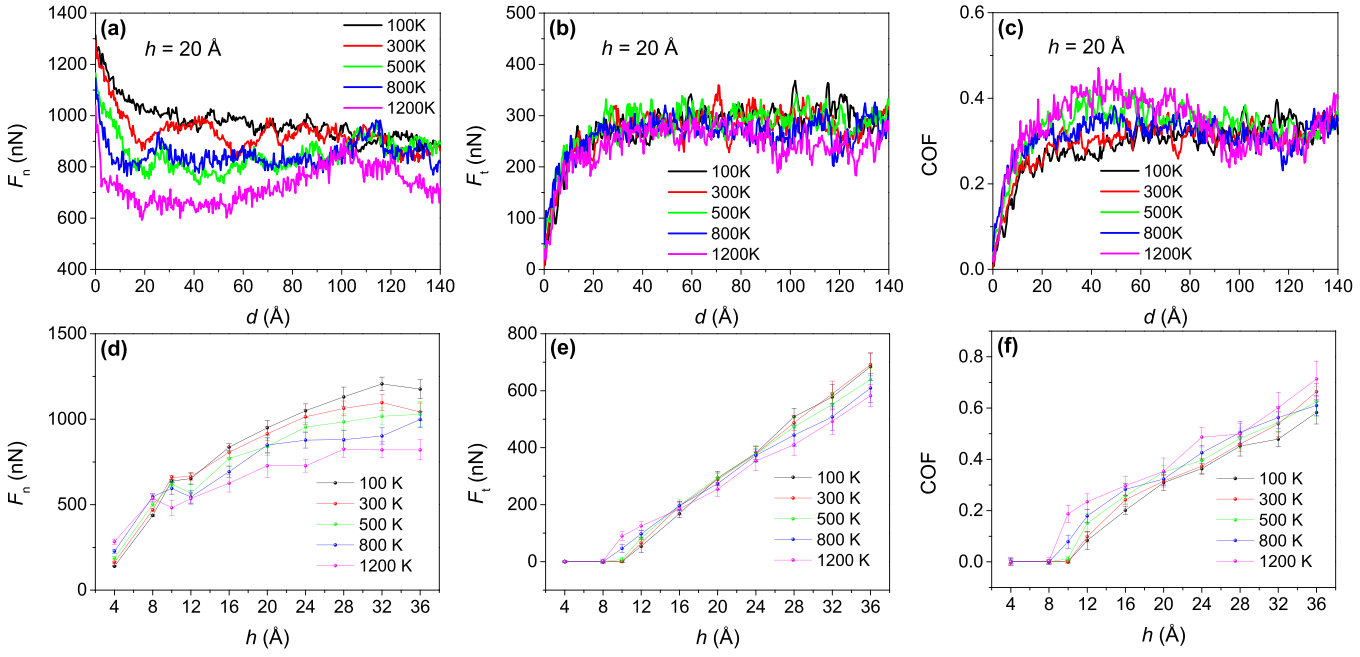

Fig. 1. Evolutions of **(a)** normal force, **(b)** tangential force, and **(c)** coefficient of friction with scratching distance for a scratching depth of $h = 20$ Å. Averaged **(d)** normal force, **(e)** tangential force, and **(f)** coefficient of friction as a function of scratching depth.

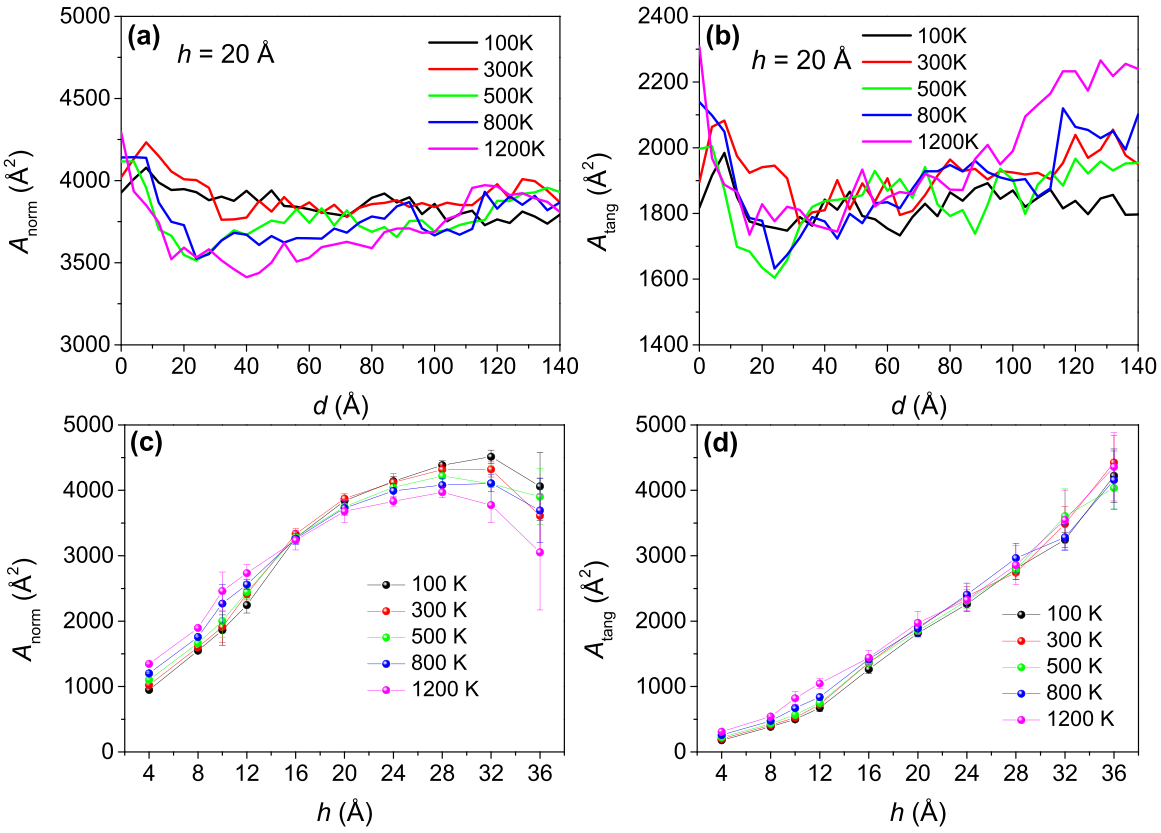

Fig. 2. Evolutions of **(a)** normal and **(b)** tangential contact areas with scratching distance for a scratching depth of $h = 20$ Å. Averaged **(c)** normal and **(d)** tangential contact areas as a function of scratching depth.

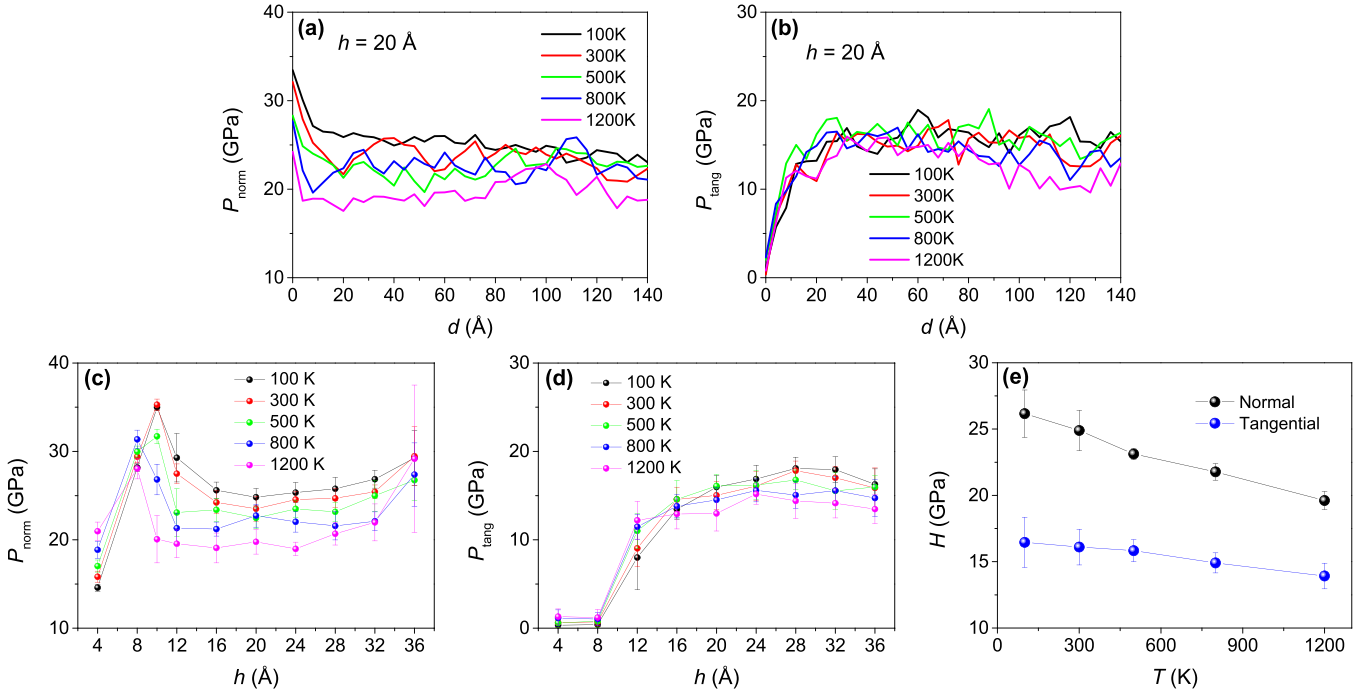

Fig. 3. Evolutions of **(a)** normal and **(b)** tangential contact pressures with scratching distance for a scratching depth of $h = 20$ Å. Averaged **(c)** normal and **(d)** tangential contact pressures as a function of scratching depth. **(e)** Averaged scratching hardness vs. temperature.

pressure with the scratching depth passed through the following stages regardless of the temperature: (I) Elastic stage, P_{norm} increased linearly with the scratching depth and P_{tang} kept very small at this stage; the high the temperature, the greater the P_{norm} and P_{tang}. (II) Elastic-plastic transition stage, P_{norm} decreased and P_{tang} increased at this stage. (III) Plastic stage, the P_{norm} and P_{tang} level off on the whole with certain

fluctuates, which conforms to the plasticity theory that in the plastic domain the contact pressure will remain unchanged and the increasing normal force can only be sustained by increasing the contact area. (IV) Ductile-brittle stage, the ductile-brittle transition occurred in AlN and it led to an evident increase in P_{norm} and a slight decrease in P_{tang}. The average value over the contact pressure in the steady plastic domain (h = 12–28 Å) is denoted as the material hardness. Variation of the normal and tangential hardness of AlN with temperature shown in Fig. 3e indicates that increasing temperature can reduce the hardness of AlN; the normal hardness decrease much faster with temperature than the tangential one is mainly due to a stronger influence of temperature on normal force and contact area. In addition, these results indicate that temperature can exhibit an influence on the elastic-plastic and ductile-fracture transition of AlN crystal, that is, the critical scratching depth and normal force to cause these transitions vary with temperature.

3.2. Influence of temperature on surface wear

Fig. 4 displays the surface morphologies and cross-sectional profiles of AlN after scratching under plastic (h = 20 Å) and ductile-brittle transition (h = 36 Å) removal situations, respectively. When h = 20 Å, evident surface wear and subsurface damage consisting of stack fault and amorphization occurred. As h increased to 36 Å, the surface wear and the pile-up, as well as the subsurface damage, became much more serious than that at 20 Å. The surface pile-up became increasingly obvious as increasing the temperature both for h = 20 Å and h = 36 Å.

The number of worn atoms (N), which has been regarded as an important parameter to evaluate nanoscale to atomic-scale wear behaviors in the MD study [47], was recorded in the scratching process. Here, the atom whose displacement amplitude exceeds twice the bond length of AlN (~1.91 Å) and did not belong to any crystal structure was defined as the worn atom. As F_n increased, the number of worn atoms stayed almost zero at first (elastic stage) and then gradually increased (plastic stage). Fig. 5 shows the variation of the number of worn atoms with F_n in the plastic removal mode [48] at different temperatures,

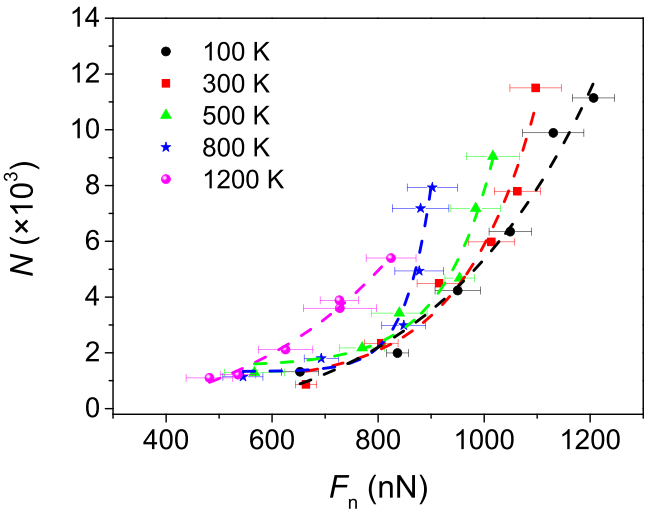

Fig. 5. Number of worn atoms vs. normal force for different temperatures.

indicating that the worn atoms increased with the increase of temperature when F_n is constant. The fitting of these data points suggests that the number of worn atoms varied exponentially with F_n and the 1200 K case is much more linear. The increasing rate can be facilitated by environmental temperatures ranging from 100 to 800 K, primarily due to that the increase in temperature can reduce the hardness of AlN (see Fig. 3e).

In the h range of 12–32 Å, the material removal of the AlN surface was dominated by plastic deformation. The specific wear rate w_s, calculated under different environmental temperature conditions according to h, as a function of F_n, was plotted in Fig. 6a. As F_n increases, w_s increases; and for the same F_n, the higher the temperature, the larger the w_s value. Moreover, w_s and F_n exhibit a significant linear correlation,

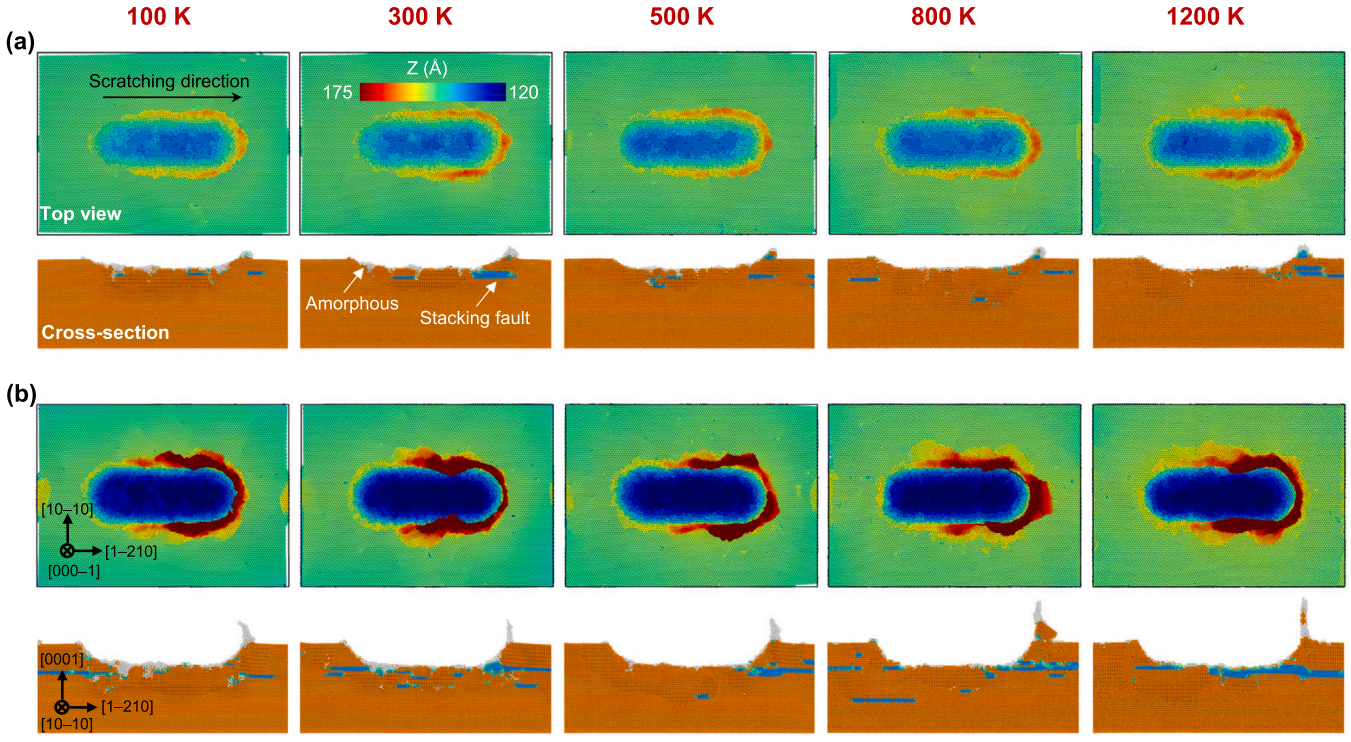

Fig. 4. Surface and cross-sectional topographies of AlN workpiece scratched by a diamond abrasive with scratching depths of **(a)** h = 20 Å and **(b)** h = 36 Å at different temperatures. These snapshots were obtained when the diamond abrasive withdrew to its initial position. The slice thickness along [10] direction for these cross-sectional profiles is 20 Å.

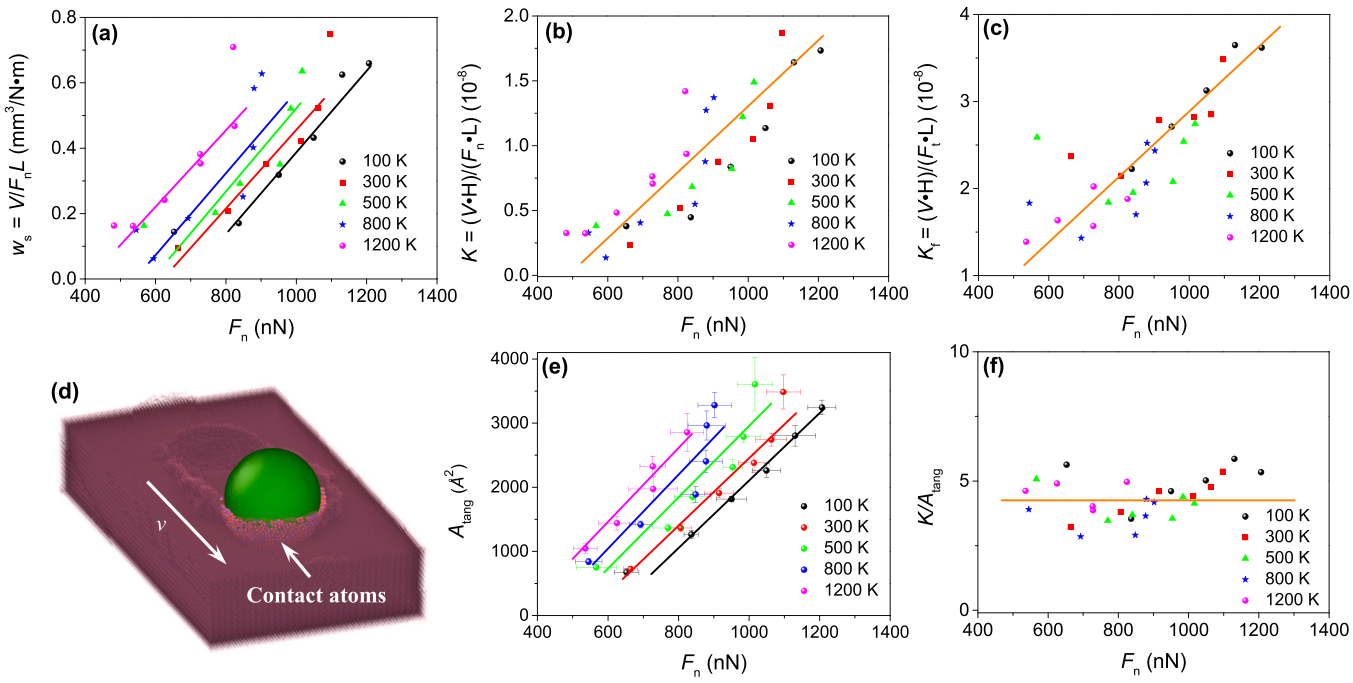

Fig. 6. **(a)** w_s, **(b)** K, **(c)** K_f of AlN substrate against diamond nano abrasive as a function of normal force at different environment temperatures. **(d)** Scratching morphology showing contact atoms and tangential contact area A_{tang} during material removal. **(e)** A_{tang}, and **(f)** K/A_{tang} as a function of normal force at different environment temperatures.

with very similar slopes of the calculated fitted lines for different temperatures. As the temperature increases, the fitted lines between w_s and F_n shift to the right. The results indicate that environmental temperature only increases w_s, but has little influence on the growth rate/slope of w_s as increasing F_n. Owing to the computational available of MD simulation, there is the capability to estimate the specific hardness values of contacting surface from the calculated scratching hardness at loading conditions and certain environmental temperatures (see Fig. 3e). According to Archard's equation (Eq. 1), K values corresponding to each F_n in the plastic domain under environmental temperature were given in Fig. 6b. In this case, the effect of temperature-induced change in surface hardness on removal behavior is excluded, and the linearity of all K values estimated at different temperatures with respect to F_n is significantly demonstrated. This indicates that temperature has almost no influence on the K value and that the decrease in hardness due to increased temperature is the crucial reason for the rise in material removal of AlN.

Furthermore, the role of frictional energy was not considered in early Archard's equation, which was subjectively and empirically assumed to be proportional to the normal force. As shown in Fig. 6c, the wear coefficient K_f, based on the modified Archard's equation with Reye's hypothesis, and F_n suggests a linear relationship with a lower statistical dispersion than the linear fitting in Fig. 6b. The simulated results demonstrate that the material removal of AlN against single diamond nanoparticle is governed by the temperature-dependent hardness of scratching area and work done at the sliding interface. Interestingly, the K_f increases linearly with the increasing F_n, independently of the environmental temperature. Based on the previous argument, the K factor is interpreted as a probability of forming wear debris from asperity encounters. In adhesive wear, the wear coefficient is used to indicate the state of wear, e.g. to characterize the transition from plastic flow/no observable wear to groove wear. Based on the hypothesis by Frérot et al. that there is a critical area A^* for the process of debris formation: if the area A of a cluster or asperity is larger than A^*, a wear particle is formed [13]. Under a certain range of loads with multi-asperities contact, K varies invariably with F_n due to the linear relationship between the wear rate and the actual contact area. The increase in the actual contact area is reflected in the increase in the number of effective asperities for the debris formation, while the effect of the increase in the contact area of a single asperity is negligible. In single asperity contact, abrasive wear is inevitable when the average applied pressure reaches $H/3$ [49]. The physical meaning of the wear factor is no longer suitable for interpretation as the probability of detachment of the substrate material, but rather as the effective contact area that can lead to material removal. Thus, the wear coefficient depends on the load. As shown in Fig. 6d, the tangential contact area (A_{tang}), represented by atomic form, of the diamond nano abrasive to AlN substrate contributes to the material removal process directly. Fig. 6e plots the calculated A_{tang} as a function of applied normal force under different environment temperatures. The results show that A_{tang} scales linearly with the normal force, and the slope varies over a small range for different temperatures. We define a dimensionless parameter as the wear coefficient normalized by tangential contact area (K/A_{tang}), which indicates the normalized removal efficiency of AlN against diamond nano abrasive. Fig. 6 f displays the approximately constant value of K/A_{tang}, which is only related to the intrinsic material properties and independent of normal force and environmental temperature. Moreover, to investigate the influence of the radius of diamond abrasive on the material removal behavior of AlN substrate, the removal process against a diamond abrasive with a radius of 70 Å was simulated, and the removal volume as a function of the applied normal force was calculated, as shown in Supplementary Fig. S8. The results display that K becomes a constant parameter independent of the load due to the limited variation of A_{tang} with increasing normal force, which is similar to the adhesive wear process. However, the underlying mechanism is still unclear, further discussion will be held in the future.

3.3. Influence of temperature on subsurface damage

Figs. 7 and 8 display snapshots of the subsurface damage of monocrystalline for $h = 20$ Å and $h = 36$ Å, respectively. The subsurface damage mainly consisted of dislocation, stack default, and amorphization. Dislocation slip is considered as the dominant mechanism of plasticity in AlN [50,51]. The dislocation with the Burget vector of $1/3 < 1\text{–}210 >$ and $1/3 < 10\text{–}10 >$ takes up the vast majority. To

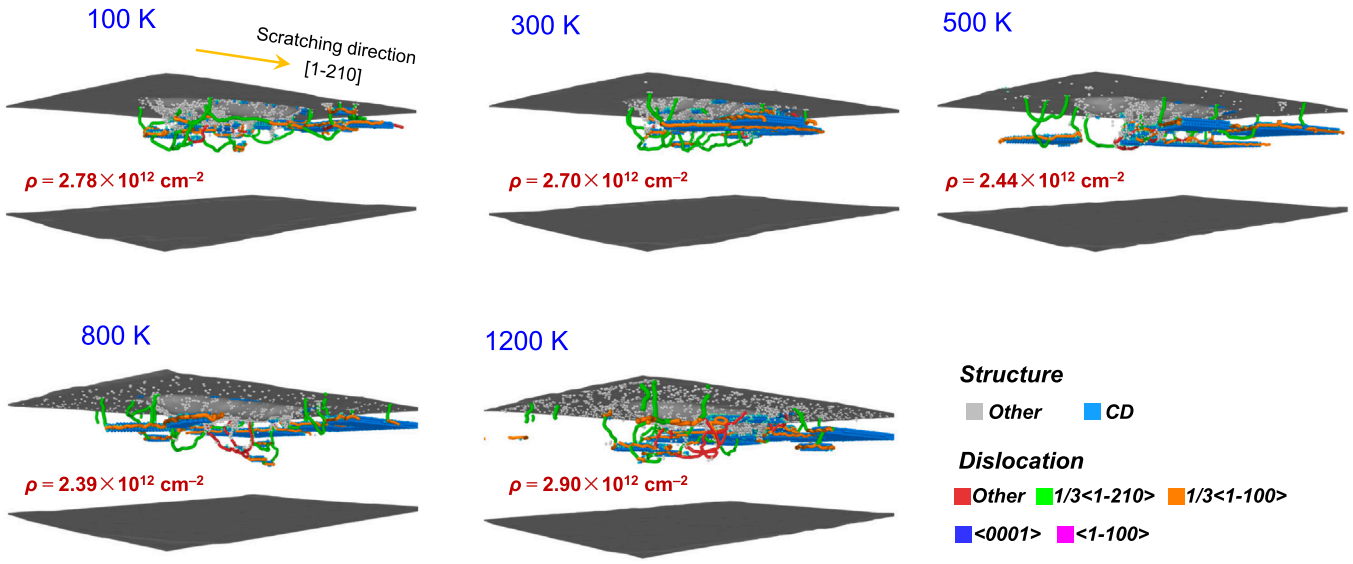

Fig. 7. The scratching-induced damage in the subsurface for the scratching depth of 20 Å at different temperatures of 100, 300, 500, 800, and 1200 K. Atoms without lattice defects are hidden in this figure.

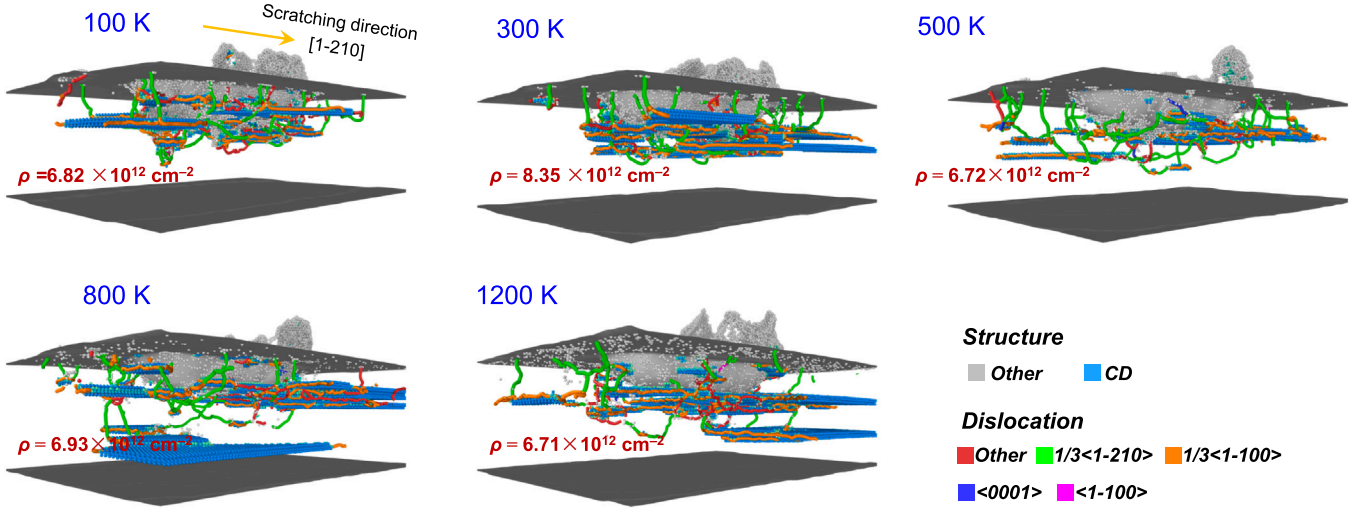

Fig. 8. The scratching-induced damage in the subsurface for the scratching depth of 36 Å at different temperatures of 100, 300, 500, 800, and 1200 K. Atoms without lattice defects are hidden in this figure.

clarify the influence of temperature on the number of dislocations, the dislocation density ρ defined as the total length of the dislocation lines divided by the volume of the Newtonian layer in the AlN workpiece was calculated [52,53]. For a given $h = 20$ Å, the dislocation density (2.9×10^{12} cm^{-2}) at 1200 K was the highest and the dislocation density (2.44×10^{12} cm^{-2}) at 500 K was the lowest at all the selected temperatures. The maximum dislocation density (8.35×10^{12} cm^{-2}) was at 300 K and the minimum dislocation density (6.71×10^{12} cm^{-2}) was at 1200 K for $h = 36$ Å. In addition, we noted that temperature can to some extent influence the dislocation network, the 'u'-shaped half dislocation loop reduced as the temperature increased.

3.4. Critical threshold of atomic removal for different temperature

Understanding the removal mechanism of monocrystalline AlN at the atomic level, and thereby clarifying the minimum removal depth and corresponding critical conditions, are of great significance in extreme manufacturing of AlN-similar hard-brittle materials at atomic/near-atomic scale [54,55]. The critical h or F_n to cause the sub/nano-scale wear of AlN differed considerably among different temperatures. In other words, minimum h or F_n to cause elastic-plastic transition (onset of plasticity) was speculated to be different at different temperatures. Fig. 9 shows the scratching-induced deformation of the AlN workpiece at different temperatures under the same $h = 10$ Å. To study the removal behavior of AlN at the atomic level, the atomic configuration involved in the bond of Al—N and the CN values for every atom were given in this figure. Fig. 9a shows the cross-sectional lattice configuration at the moment when d reached 70 Å. The atom according to CN value exhibited a regular distribution for the temperatures of 100 K and 300 K, in which the CN value for the deformation region was primary five, indicating a compression-induced phase with a fivefold-coordinated hexagonal structure. Contrastively, the distribution for greater temperatures of 500, 800, and 1200 K became less regular. The temporary compression-induced phase transition with CN ≥ 5 can be eliminated after unloading. For the cases of 100–500 K temperature conditions, the deformed AlN recovered to its pristine wurtzite lattice structure entirely after the diamond abrasive withdrew from the AlN substrate, suggesting such deformation was the complete elastic one. As the temperature

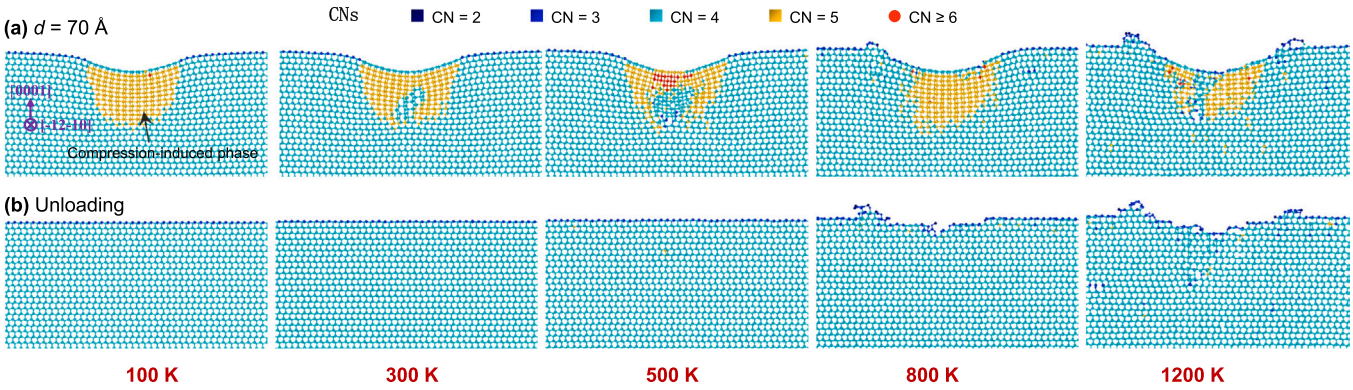

Fig. 9. Atomic structure with bonding configuration of AlN workpiece scratched with a scratching depth of $h = 10$ Å at different temperatures. **(a)** Snapshots when the scratching distance $d = 7$ nm. **(b)** Snapshots when the diamond abrasive withdrawing from the AlN workpiece. Atoms are colored according to their CN values.

increased to 800 K and 1200 K, evident plasticity-dominated material removal took place on the scratching track. The removal depth was equal to a monolayer of AlN for 800 K, whereas a three-step structure for 1200 K in which the thickness of each layer was exactly a monolayer of AlN. In addition, many point defects including vacancies and interstitials were observed in the subsurface at 1200 K mainly due to the drastic thermal motion at high temperature.

To further clarify the critical h or F_n to cause surface wear and the minimum removal depth for different temperatures, a series of h values within the elastic-plastic transition regime was selected to carry out the additional scratching simulation. The results were listed in Table 3. The threshold h to cause the wear of AlN at the temperature of 100, 300, 500, 800, and 1200 K is 11.6, 11.2, 10.6, 9.6, and 8.2 Å, respectively. Correspondingly, the critical F_n to cause the wear of monocrystalline AlN decreased from ~670 to ~484 nN with the increase of temperature from 100 to 1200 K, as shown in Fig. 10a.

The entire surface morphologies and local cross-sectional profiles of the wear track caused by scratching under the critical h, as well as the variation of tangential force with d in the scratching process for these temperatures, are shown synthetically in Fig. 10b and c. Changes in the tangential force are associated with the wear of AlN. The tangential force was kept low when the wear did not occur and once d reached a certain value and the wear occurred, there was a steep increase in tangential force. This moment also corresponded to the nucleation of the dislocation that was the onset of plastic deformation of the AlN crystal, which demonstrates once again that dislocation glide behavior is the leading mechanism of AlN plastic deformation at the nanoscale. On the other hand, the surface wear morphology varied evidently with the temperature.

The wear track at low temperatures was longer than that at high temperatures. For example, the wear track at 800 and 1200 K is only half of the maximum scratching distance of 140 Å, and the minimum removal depth for these temperatures all equaled a monolayer AlN layer, but the wear morphology exhibited some difference. The monolayer removal of AlN was realized along the entire wear track for the temperature of 100 K along with the flattest wear surface. The subsurface defects increased significantly at 300 K temperature. The removal depth of 500, 800, and 1200 K was equal to a double layer of AlN at the beginning, and then to one layer only. In the process of the change from a double layer to a single layer, the tangential force also showed a downward trend, which is related to the decrease in the actual scratching depth. In addition, there are plenty of defects in the subsurface under ultrahigh temperature conditions (800–1200 K) due to the intensified thermal motion of atoms.

4. Conclusion

In this work, temperature-dependent material removal behaviors of single-crystal AlN from the nanoscale to atomic scale at a wide range of scratching depths are investigated using MD simulation. the main conclusions are as follows:

(1) AlN crystal goes through elastic, plastic, and brittle fracture stages with the increase in scratching depth regardless of temperature. The changes in terms of elastic-plastic and ductile-brittle transitions can be captured from the curves of forces, contact area, and contact pressure versus scratching depth. In the steady plastic stage, the higher the temperature, the larger the coefficient of friction, primarily due to that the influence of temperature on the normal force is greater than the tangential force. The number of worn atoms increases exponentially with the normal force in the plastic domain. In addition to the temperature of 1200 K, the higher the temperature, the higher the increasing rate, which is associated with the decrease in the hardness of AlN.

(2) The material removal value of AlN as a function of the normal force was estimated and K values for different temperatures were calculated based on the Archard-type equation. K scales linearly as the increasing normal force, and the slope is independent of temperature, which indicates that the temperature facilitation of AlN material removal is mainly attributed to the reduction of hardness. Independently of normal force and temperature, a normalized wear coefficient, K/A_{tang}, is developed to interpret the removal efficiency of AlN substrate with diamond abrasive.

(3) The critical conditions, i.e., scratching depth and normal force to cause near-atomic wear of single-crystal AlN are temperature dependent. The higher the temperature, the smaller the critical scratching depth and normal force. A minimum removal depth with monolayer of AlN is achieved under the present simulation conditions at every temperature, whereas the surface wear patterns and subsurface lattice damage vary greatly when the critical wear occurs at different

Table 3
Critical parameters to cause wear of AlN for different temperatures.

T (K)	100	300	500	800	1200
h (Å)	11.6	11.2	10.6	9.6	8.2
F_n (nN)	670 ± 42	622 ± 23	580 ± 49	535 ± 55	484 ± 57
F_t (nN)	58 ± 13	47 ± 11	50 ± 24	38 ± 23	38 ± 27
COF	0.087 ± 0.02	0.076 ± 0.02	0.089 ± 0.04	0.076 ± 0.04	0.085 ± 0.06

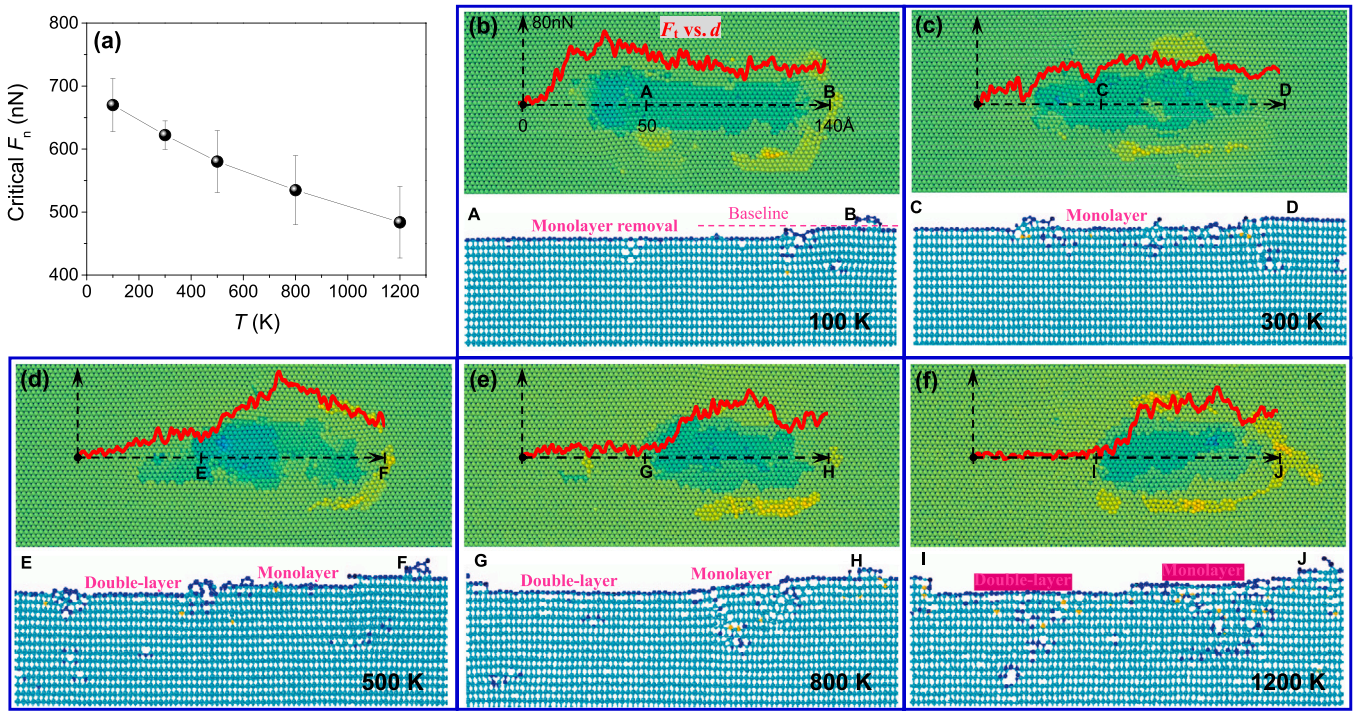

Fig. 10. **(a)** Critical normal force to cause wear. **(b)** — **(f)** Surface wear with a minimum removal depth for different temperatures of 100, 300, 500, 800, and 1200 K.

temperatures. The onset of wear corresponds well to the generation of dislocation, suggesting that the dislocation slide is the crucial factor to cause plasticity-dominated removal of AlN crystal.

5. Statement of Originality

I would like to declare on behalf of my co-authors that the work described was original research that has not been published previously, and not under consideration for publication elsewhere, in whole or in part.

CRediT authorship contribution statement

Jian Guo: Conceptualization, Investigation, Data curation, Formal analysis, Writing – original draft, Supervision, Funding acquisition. **Yang Liu:** Methodology, Investigation. **Lingfeng Duan:** Investigation, Visualization. **Fengling Zhang:** Investigation, Formal analysis. **Chen Xiao:** Project administration, Conceptualization, Investigation, Data curation, Writing – review & editing, Supervision**.** All authors have read and approved the manuscript.

Declaration of Competing Interest

The authors declare that they have no known competing financial interests or personal relationships that could have appeared to influence the work reported in this paper.

Data Availability

Data will be made available on request.

Acknowledgments

This work was well supported by the National Natural Science Foundation of China (No. 51805240) and the Scientific Research Foundation of University of South China. We would like to acknowledge the HPC Center of University of South China in running the LAMMPS software.

Appendix A. Supporting information

Supplementary data associated with this article can be found in the online version at doi:10.1016/j.triboint.2023.108575.

References

[1] Bhushan B, Israelachvili JN, Landman U. Nanotribology: friction, wear and lubrication at the atomic scale. Nature 1995;374:607–16.
[2] Xiao C, Hsia F-C, Sutton-Cook A, Weber B, Franklin S. Polishing of polycrystalline diamond using synergies between chemical and mechanical inputs: a review of mechanisms and processes. Carbon 2022;196:29–48.
[3] Vakis AI, Yastrebov VA, Scheibert J, Nicola L, Dini D, Minfray C, et al. Modeling and simulation in tribology across scales: an overview. Tribol Int 2018;125:169–99.
[4] Kim SH, Asay DB, Dugger MT. Nanotribology and MEMS. Nano Today 2007;2:22–9.
[5] Bhushan B. Nanotribology and nanomechanics of MEMS/NEMS and BioMEMS/BioNEMS materials and devices. Microelectron Eng 2007;84:387–412.
[6] Zhang J, Jiang Y, Luo H, Yin S. Prediction of material removal rate in chemical mechanical polishing via residual convolutional neural network. Control Eng Pract 2021:107.
[7] Marian M, Tremmel S. Current trends and applications of machine learning in tribology-a review. Lubricants 2021:9.
[8] Kato K. Classification of wear mechanisms/models. Proc Inst Mech Eng Part J-J Eng Tribol 2002;216:349–55.
[9] Archard JF. Contact and rubbing of flat surfaces. J Appl Phys 1953;24:981–8.
[10] Guo J, Tan S, Xiao C. Atomistic understanding of scratching-induced material attrition of wurtzite single-crystal AlN using nanoscale diamond abrasive. Tribol Int 2022;169:107483.
[11] Xie YS, Bhushan B. Fundamental wear studies with magnetic particles and head cleaning agents used in magnetic tapes. Wear 1996;202:3–16.
[12] Brink T, Frerot L, Molinari J-F. A parameter-free mechanistic model of the adhesive wear process of rough surfaces in sliding contact. J Mech Phys Solids 2021:147.
[13] Frerot L, Aghababaei R, Molinari J-F. A mechanistic understanding of the wear coefficient: From single to multiple asperities contact. J Mech Phys Solids 2018;114:172–84.
[14] Guo J, Xiao C, Gao J, Li G, Qian L. Interplay between counter-surface chemistry and mechanical activation in mechanochemical removal of N-faced GaN surface in humid ambient. Tribology Int 2021;159:107004.
[15] Xiao C, Guo J, Zhang P, Chen C, Chen L, Qian L. Effect of crystal plane orientation on tribochemical removal of monocrystalline silicon. Sci Rep 2017:7.

[16] Celano U, Hsia F-C, Vanhaeren D, Paredis K, Nordling TEM, Buijnsters JG, et al. Mesoscopic physical removal of material using sliding nano-diamond contacts. Sci Rep 2018:8.
[17] Xiao C, Li J, Guo J, Zhang P, Yu B, Chen L, et al. Role of mechanically -driven distorted microstructure in mechanochemical removal of silicon. Appl Surf Sci 2020:520.
[18] Zhou C-G, Ou Y, Feng H-T, Chen Z-T. Investigation of the precision loss for ball screw raceway based on the modified Archard theory. Ind Lubr Tribology 2017;69:166–73.
[19] Liu Y, Zhu D, Gilbert JL. Sub-nano to nanometer wear and tribocorrosion of titanium oxide-metal surfaces by in situ atomic force microscopy. Acta Biomater 2021;126:477–84.
[20] Ma H, Bennewitz R. Nanoscale friction and growth of surface oxides on a metallic glass under electrochemical polarization. Tribol Int 2021;158(14):106925.
[21] Guo J, Xiao C, Gao J, Liu J, Chen L, Qian L. Effect of native oxide layer on mechanochemical reaction at the GaN–Al_2O_3 interface. Front Chem 2021:9.
[22] Harrison J. Atomic-scale simulation of tribological and related phenomena. Handb Micro/Nano Tribol 1995:525.
[23] Srivastava I, Kotia A, Ghosh SK, Ali MKA. Recent advances of molecular dynamics simulations in nanotribology. J Mol Liq 2021;335:116154.
[24] Pearson SR, Shipway PH, Abere JO, Hewitt RAA. The effect of temperature on wear and friction of a high strength steel in fretting. Wear 2013;303:622–31.
[25] Liu Z, Gong J, Xiao C, Shi P, Kim SH, Chen L, et al. Temperature-dependent mechanochemical wear of silicon in water: the role of Si-OH surfacial groups. Langmuir 2019;35:7735–43.
[26] Torres H, Varga M, Adam K, Ripoll MR. The role of load on wear mechanisms in high temperature sliding contacts. Wear 2016;364:73–83.
[27] Yang N, Huang W, Lei D. Control of nanoscale material removal in diamond polishing by using iron at low temperature. J Mater Process Technol 2020:278.
[28] Norris JA, Stabile KJ, Jinnah RH. An introduction to tribology. J Surg Orthop Adv 2008;17:2–5.
[29] Sakkaki M, Moghanlou FS, Vajdi M, Pishgar F, Shokouhimehr M, Asl MS. The effect of thermal contact resistance on the temperature distribution in a WC made cutting tool. Ceram Int 2019;45:22196–202.
[30] Yamamoto S, Liskiewicz T, Fujimura K, Tashiro K, Takai O. Temperature rise of diamond-like carbon during sliding: Consideration of the real contact area. Tribol Int 2019;131:496–507.
[31] Qin W, Jin X, Kirk A, Shipway PH, Sun W. Effects of surface roughness on local friction and temperature distributions in a steel-on-steel fretting contact. Tribol Int 2018;120:350–7.
[32] Oestringer LJ, Proppe C. On the transient thermomechanical contact simulation for two sliding bodies with rough surfaces and dry friction. Tribol Int 2022:170.
[33] Zhang L, Yuan J, He S, Huang S, Xiong S, Shi T, et al. Contact heat transfer analysis between mechanical surfaces based on reverse engineering and FEM. Tribol Int 2021:161.
[34] Bondokov RT, Branagan SP, Ishigami N, et al. Two-inch aluminum nitride (AIN) single crystal growth for commercial applications. ECS Trans 2021;104(7):37–48.
[35] Ganji MD, Dalirandeh Z, Khorasani M. Lithium absorption on single-walled boron nitride, aluminum nitride, silicon carbide and carbon nanotubes: a first-principles study. J Phys Chem Solids 2016;90:27–34.
[36] Iqbal A, Mohd-Yasin F. Reactive sputtering of aluminum nitride (002) thin films for piezoelectric applications: a review. Sensors 2018:18.
[37] Zagorac J, Zagorac D, Jovanovic D, Lukovic J, Matovic B. Ab initio investigations of structural, electronic and mechanical properties of aluminum nitride at standard and elevated pressures. J Phys Chem Solids 2018;122:94–103.
[38] Li N., Ho C.P., Cao Y., Zhu S., Chen G.F.R., Fu Y.H., et al. Aluminum Nitride Photonics Platforms on Silicon Substrate. Conference on Lasers and Electro-Optics (CLEO). Electr Network 2021.
[39] Kang HS, Lee JH, Park JH, Lee HA, Park WI, Kang SM, et al. Optimization of the CMP process with colloidal silica performance for bulk MN single crystal substrate. Korean J Met Mater 2019;57:582–8.
[40] Vashishta P, Kalia RK, Nakano A, Rino JP. Interaction potential for silicon carbide: a molecular dynamics study of elastic constants and vibrational density of states for crystalline and amorphous silicon carbide. J Appl Phys 2007;101:217–340.
[41] Schneider T, Stoll E. Molecular-dynamics study of a three-dimensional one-component model for distortive phase transitions. Phys Rev B 1978;17:1302.
[42] Stukowski A, Bulatov VV, Arsenlis A. Automated identification and indexing of dislocations in crystal interfaces. Model Simul Mater Sci Eng 2012;20(8):1–16.
[43] Williams BE, Glass JT. Characterization of diamond thin films: diamond phase identification, surface morphology, and defect structures. J Mater Res 2011;4:373–84.
[44] Stukowski A. Visualization and analysis of atomistic simulation data with OVITO–the open visualization tool. Model Simulmaterscieng 2010;18:2154–62.
[45] Alhafez IA, Brodyanski A, Kopnarski M, Urbassek HM. Influence of tip geometry on nanoscratching. Tribol Lett 2017:65.
[46] Avila KE, Kuechemann S, Alhafez IA, Urbassek HM. Nanoscratching of metallic glasses – an atomistic study. Tribol Int 2019;139:1–11.
[47] Bai L, Srikanth N, Korznikova EA, Baimova JA, Dmitriev SV, Zhou K. Wear and friction between smooth or rough diamond-like carbon films and diamond tips. Wear 2017;372–373:12–20.
[48] Zhang T, Jiang F, Huang H, Lu J, Wu Y, Jiang Z, et al. Towards understanding the brittle–ductile transition in the extreme manufacturing. Int J Extrem Manuf 2021;3:022001.
[49] Burwell JT, Strang CD. On the empirical law of adhesive wear. J Appl Phys 1952;23:18–28.
[50] Xiang H, Li H, Tao F, Zhao Y, Peng X. Molecular dynamics simulation of AlN thin films under nanoindentation. Ceram Int 2016;43:138–45.
[51] Li B, Li J, Zhu P, Xu J, Li R, Yu J. Influence of crystal anisotropy on deformation behaviors in nanoscratching of AlN. Appl Surf Sci 2019;487:1068–76.
[52] Fan YH, Wang WY, Hao ZP, Zhan CY. Work hardening mechanism based on molecular dynamics simulation in cutting Ni–Fe–Cr series of Ni-based alloy. J Alloy Compd 2020;819:153331.
[53] He SH, He BB, Zhu KY, Huang MX. Evolution of dislocation density in bainitic steel: Modeling and experiments. Acta Mater 2018;149:46–56.
[54] Wu YQ, Mu DK, Huang H. Deformation and removal of semiconductor and laser single crystals at extremely small scales. Int J Extrem Manuf 2020;2(1):012006.
[55] Fang FZ. Atomic and close-to-atomic scale manufacturing: perspectives and measures. Int J Extrem Manuf 2020;2(3):030201.